https://doi.org/10.5194/amt-2019-184
Preprint. Discussion started: 19 June 2019

Atmospheric Measurement Techniques Discussions

Molecular Characterization of Alkyl Nitrates in Atmospheric Aerosols by Ion Mobility Mass Spectrometry

Xuan Zhang[1,*], Haofei Zhang[2,3], Wen Xu[4], Geoffrey S. Tyndall[1], John J. Orlando[1], John T. Jayne[4], Douglas R. Worsnop[4], and Manjula R. Canagaratna[4,*]

[1] Atmospheric Chemistry Observation & Modeling Laboratory, National Center for Atmospheric Research, Boulder, CO 80301, USA
[2] Department of Chemistry, University of California, Riverside, CA 92521, USA
[3] Environmental Toxicology Program, University of California, Riverside, CA 92521, USA
[4] Center for Aerosol and Cloud Chemistry, Aerodyne Research Inc., Billerica, MA 01821, USA

Correspondence to: Xuan Zhang (xuanz@ucar.edu)
Manjula R. Canagaratna (mrcana@aerodyne.com)

https://doi.org/10.5194/amt-2019-184
Preprint. Discussion started: 19 June 2019

Atmospheric Measurement Techniques Discussions

Abstract

We demonstrate the capability of the Ion Mobility Mass Spectrometry (IMS-MS) for molecular characterization of reactive and short-lived alkyl nitrates (ANs) in atmospheric aerosols. We show significantly enhanced production of ion adducts from a selection of alkyl nitrates by clustering with inorganic anions such as chloride and nitrate during negative electrospray, a special chemical ionization mechanism in the condensed phase. This approach enables the detection of ANs that have low tendency to form molecular ions on their own by electrospray ionization. Molecular identity of each AN adduct is well constrained by the developed collision cross section vs. mass to charge ratio correlation, which provides a two-dimensional separation of the $-ONO_2$ containing compounds on the basis of their molecular size and geometry. Structural information of AN molecules is further probed by the identification of characteristic fragments produced from the collision induced dissociation of parent AN adducts. Application of the IMS-MS technique is exemplified by the identification of hydroxy nitrates in secondary organic aerosols produced from isoprene photochemistry.

https://doi.org/10.5194/amt-2019-184
Preprint. Discussion started: 19 June 2019

Atmospheric Measurement Techniques Discussions

1. Introduction

Alkyl nitrates (ANs; ANs = $RONO_2$) constitute a major fraction and serve as a temporary reservoir of total reactive nitrogen oxides in the atmosphere (Perring et al., 2013). ANs are primarily produced from the hydroxyl radical (OH) initiated oxidation of volatile organic compounds (VOCs) in the presence of nitrogen oxides (NO_x) during daytime and the nitrate radical (NO_3) initiated oxidation of alkenes during nighttime. Once formed, ANs are primarily subjected to further chemical transformation leading to the recycling of NO_x, partitioning into the particle phase forming secondary organic aerosols (SOA), or deposition resulting in the loss of atmospheric NO_x. Characterization of alkyl nitrates is of crucial importance in understanding regional NO_x budget, tropospheric ozone production, as well as chemical mechanisms leading to the SOA formation (Brown et al., 2009; Farmer et al., 2011; Rollins et al., 2012; Rosen et al., 2004).

A suite of analytical techniques, such as thermal dissociation laser-induced-fluorescence spectroscopy (TD-LIF) (Thornton et al., 2000; Day et al., 2002; Wooldridge et al., 2010), chemical ionization mass spectrometry (CIMS) (Beaver et al., 2012; Loza et al., 2014; Krechmer et al., 2015; Nguyen et al., 2015; Schwantes et al., 2015; Teng et al., 2015; Xiong et al., 2015; Schwantes et al., 2017), and gas chromatography coupled with electron capture detection (GC-ECD) (Atlas, 1988; O'Brien et al., 1995), have been employed for *in situ* measurement of total and individual ANs in the gas phase. Observations of ANs in the particle phase, however, are rather limited due to the intensive denitrification during the preparation and analysis of particle samples. Efforts have been made to characterize the total amount of ANs and the number of $–ONO_2$ functional groups using TD-LIF and Fourier transform infrared spectroscopy (FTIR) (Rollins et al., 2010; Russell et al., 2011). The NO_2^+ / NO^+ ratio derived from the aerosol mass spectrometry (AMS) measurements has also been used as an indicator for the presence of alkyl nitrates in submicrometer particles (Farmer et al., 2010; Kiendler-Scharr et al., 2016; Xu et al., 2017). These techniques have provided important insights into the prevalence and abundance of ANs in atmospheric aerosols, although the molecular information of individual ANs is lacking. Recent development on the filter inlet for gases and aerosols (FIGAERO) interfaced with the CIMS instrument has allowed for on-line speciation and quantification of functionalized alkyl nitrates in the particle phase (Lee et al., 2016). While the molecular composition of any given compounds can be inferred from the mass spectra, structural information on isomeric and

https://doi.org/10.5194/amt-2019-184
Preprint. Discussion started: 19 June 2019


Atmospheric Measurement Techniques Discussions

63 isobaric species that are commonly produced from atmospheric chemical transformation
64 is not available from CIMS measurements.

65 In this study, we present the first demonstration of the Ion Mobility Mass
66 Spectrometry (IMS-MS) interfaced with an Electrospray Ionization (ESI) source for the
67 molecular characterization of alkyl nitrates in the condensed phase. We show the
68 significant production of AN clusters of the form $[M+Cl]^-$, $[M+NO_3]^-$, $[M+I]^-$, and
69 $[M+Ac]^-$, respectively, with selected anions including chloride, nitrate, iodide, and
70 acetate. The anion attachment represents a new option for the detection of the $-ONO_2$
71 functionality that is unlikely to produce measurable amount of molecular ions on its own
72 during ESI. The optimal anion concentration to essentially promote the ion adduct
73 formation is on the order of milli-molar, which is significantly higher than the level of
74 those naturally present in ambient aerosols. We develop an intrinsic collision cross
75 section vs. mass to charge ratio correlation based on the ion mobility measurements of
76 five AN standards, providing a two-dimensional identification of unknown molecules
77 that are likely containing the $-ONO_2$ moiety. Additionally, the molecular identity of ANs
78 can be verified via the characteristic fragment produced from the collision induced
79 dissociation of the parent ion adducts. We apply the IMS-MS technique to identify ANs
80 in SOA produced from isoprene photochemistry.

81 **2. Experiments**

82 **2.1. Materials**

83 Organic nitrate and nitro standards stored in acetonitrile ampules, including 100
84 µg/mL 1-mononitroglycerin (MNG), 100 µg/mL 1,3-dinitroglycerin (DNG), 1000 µg/mL
85 pentaerythritol tetranitrate (PETN), 1000 µg/mL hexahydro-1,3,5-trinitro-1,3,5-triazine
86 (RDX), and 1000 µg/mL 2,4-dinitrotoluene (DNT), were purchased from SigmaAldrich.
87 They are further diluted with methanol (HPLC grade, J. T. Baker) to 5 µM or less. Stock
88 solutions of ammonium acetate (>99%, SigmaAldrich), ammonium chloride (>99%,
89 SigmaAldrich), sodium nitrate (>99%, SigmaAldrich), and sodium iodide (>99%,
90 SigmaAldrich) were prepared at a concentration of 10 mM in methanol. They were used
91 as additives at typical concentrations of 0.01 – 0.1 mM in the AN methanol solution to
92 facilitate ion adducts formation.

93 **2.2. Experiments**

94 SOA samples containing alkyl nitrates were generated from the OH-oxidation of
95 isoprene under high-NO_x conditions in the NCAR 10 m^3 Atmospheric Simulation

https://doi.org/10.5194/amt-2019-184
Preprint. Discussion started: 19 June 2019

Atmospheric Measurement Techniques Discussions

Chamber (Zhang et al., 2018). H_2O_2 was used as the OH source by evaporating 133 μL aqueous solution (30 wt% in water, SigmaAldrich) into the chamber with 5 L/min purified air for ~120 min, resulting in a starting concentration of ~4 ppm. Isoprene was injected into the chamber by evaporating ~17 μL liquid standard (≥99%, SigmaAldrich) with 5 L/min purified air for ~20 min, resulting an initial concentration of ~500 ppb. NO was injected into the chamber from a concentrated NO cylinder source (NO = 133.16 ppm, balance N_2) to achieve an initial concentration of ~500 ppb. Seed aerosol was injected into the chamber by atomizing 0.06 M aqueous ammonium sulfate solution to provide sufficient surface area for the partitioning of alkyl nitrates. The chamber contents were allowed to mix for ~30 min before the onset of irradiation. After ~2 hr photooxidation, NO was nearly depleted (>5 ppb) and the irradiation was ceased. SOA produced was then collected on Teflon filters (47-mm diameter, 0.5-μm pore size, MILLIPORE) through active sampling at a flow rate of 10 L/min for ~3 hr (Schilling Fahnestock et al., 2014; Zhang et al., 2014; Huang et al., 2016; Thomas et al., 2016). Filters were stored in a -20 °C freezer prior to analysis. SOA samples were extracted in 20 mL HPLC-grade methanol by 45 min of sonication at ~273 K and then concentrated to ~5 mL with the assistance of a ~2 L/min N_2 stream.

2.3. Instrumental

The Electrospray Ionization Drift-Tube Ion Mobility Spectrometer (DT-IMS) interfaced to a Time-of-Flight Mass Spectrometer (TOFMS) was utilized in the characterization of ANs. The instrument was designed and manufactured by Tofwerk (AG, Switzerland), with detailed descriptions and schematics provided by previous studies (Kaplan et al., 2010; Groessl et al., 2015; Krechmer et al., 2016; Zhang et al., 2016b; Zhang et al., 2017). Here we will present the instrument operation protocols specific to the ANs measurement.

AN standards and SOA filter extracts were delivered to the ESI source via a 250 μL gas-tight syringe (Hamilton) held on a syringe pump (Harvard Apparatus) at a flow rate of 1 μL min^{-1}. The optimal ESI potential to readily generate stable ion adducts while minimizing the corona discharge was found to be −1800 V. The negatively charged mist generated at the emitter tip is introduced into the drift tube through a Bradbury-Nielson ion gate located at the entrance with the assistant of 1 L min^{-1} nitrogen sheath gas. The BN ion gate was operated at the Hadamard Transform mode, with a closure voltage of 50 V and a gate pulse frequency of 1.2×10^3 Hz. The drift tube was held at a constant temperature (340±3 K) and atmospheric pressure (~766 *Torr*). A counter flow of N_2 drift gas was introduced at the end of the drift region at a flow rate of 1.2 mL min^{-1}. Ion

https://doi.org/10.5194/amt-2019-184
Preprint. Discussion started: 19 June 2019

Atmospheric Measurement Techniques Discussions

mobility separation was carried out at the field strength ranging from 300 to 400 V cm^{-1}. After exiting from the drift tube, ions were focused into a pressure-vacuum interface that includes two segmented quadrupoles (Q_1 and Q_2) through an ion lens and a nozzle. Note that the potential gradient applied to the ion lens and nozzle should be limited to 500 V or less to prevent intensive fragmentation of the molecular ions. The frequency and amplitude were set as 1.5×10^6 Hz and 196 V for Q_1 and 1.5×10^6 Hz and 250 V for Q_2, respectively. Collision induced dissociation (CID) can be performed by adjusting the voltages on the ion optical elements between the two quadruple stages. Over the course of a CID program, the quadrupoles were set to 1.3×10^6 Hz and 120 V for Q_1 and 1.2×10^6 Hz and 150 V for Q_2, respectively, to ensure good transmission of low masses (m/z < 100).

The ESI-IMS-TOFMS instrument was operated in the m/z range of 20 to 1500 with a total recording time of 60 s for each dataset. The mass spectrometer was calibrated using sodium nitrate, ammonium phosphate, sodium dodecyl sulfate, sodium taurocholate hydrate, and ultramark 1621 in the negative mode. The ion mobility measurements were calibrated using tetrabutyl ammonium chloride as the instrument standard and 2,4-lutidine as the mobility standard (Zhang et al., 2016b). Mass spectra and ion mobility spectra were collected by Aquility DAQ v2.1.0 and post processed by Tofware v2.5.3.

3. Results and Discussion

3.1. Ion adduct formation

The strong electron affinity of the $-ONO_2$ functional group makes alkyl nitrate a potential candidate for being analyzed in the negative electrospray ionization mode. However, the ESI(−) mass spectra of the AN standards investigated here are typically characterized by various fragments and clusters due principally to the thermally labile $-ONO_2$ moiety. As shown in Figure 1, no molecular ion ($[M]^-$ or $[M-H]^-$) is observed on the ESI(−) mass spectra of 1-mononitroglycerin (MNG), 1,3-dinitroglycerin (DNG), and pentaerythritol tetranitrate (PETN). Instead, a small peak appears as a cluster ion of the form $[M+NO_2-H]^-$. It is worth noting that addition of water to the mobile phase does not promote the molecular ion formation, rather significant nitrate losses via hydrolysis were observed. With the addition of trace amount of salts, i.e., ammonium chloride (NH_4Cl), sodium nitrate ($NaNO_3$), sodium iodide (NaI), and ammonium acetate (NH_4Ac), the overall signal intensities were significantly enhanced through the production of a suite of adduct ions of the form $[M+Cl]^-$, $[M+NO_3]^-$, $[M+I]^-$, and $[M+Ac]^-$, respectively. The relative sensitivities of individual adduct ions increase by ultimately two orders of

https://doi.org/10.5194/amt-2019-184
Preprint. Discussion started: 19 June 2019


Atmospheric Measurement Techniques Discussions

magnitude, compared with the pure standard in methanol solution. Here the observed ion adduct formation in ESI can be considered as a special case of chemical ionization occurring in solution before the charge separation process takes place.

Table 1 lists the characteristic adduct ions formed from three AN standards (MNG, DNG, and PETN) in methanol solution with selected additives (NH_4Ac, NH_4Cl, NaI, and $NaNO_3$). Ion adducts are ubiquitously observed from all of the ANs investigated, regardless of the number of $–ONO_2$ functional groups attached on the molecule. Nitrate (NO_3^-) and chloride (Cl^-) anions were found to be the most effective additives to promote ion adduct formation. Nitrate clusters exhibit the highest signal intensity and lowest limit of detection, especially for the poly-nitrates and functionalized alkyl nitrates investigated. Chloride clusters are characterized by two distinct ions with a mass difference of 2 amu and abundance ratio of 3:1 due to the natural presence of isotopes ^{35}Cl and ^{37}Cl. Also given in Table 1 are the detected negative ions from two organic nitro compounds, i.e., hexahydro-1,3,5-trinitro-1,3,5-triazine (RDX) and 2,4-dinitrotoluene (DNT). In contrast to RDX, which undergoes intensive clustering processes with Cl^-, I^-, and NO_3^- during negative ESI, one dominant molecular ion ($[M-H]^-$) was observed on the ESI(−) mass spectra of DNT.

The effect of the additive concentrations (NO_3^- and Cl^-) on the ion adduct formation was investigated using an equimolar mixture (5 μM each) of PETN and RDX as representative of nitrates and nitro compounds, respectively, in methanol solution (Figure 2). In the absence of any additives, the presence of background anions from either impurities in the solvent or thermal decomposition of alkyl nitrates leads to a detectable amount of ion adducts. With the anion levels on the order of micromolar, ion adducts become dominant in the ESI(−) mass spectra. The optimal anion concentration was found to be in the range of 0.01 mM to 0.1 mM. Progressively rising anion concentrations (> 1mM) essentially suppress adduct formation due to the competition for limited resources, such as space and charge (Cech and Enke, 2001). Note that the measured drift time for each ion adduct is consistent at anion concentrations ranging from 1 μM to 1 mM, indicative of the absence of ion-molecule clustering in the IMS drift tube.

3.2. Collision cross section vs. mass to charge ratio trend line

Collision cross section (Ω_{N_2}) represents the effective area for interactions between a charged molecule and the surrounding buffer gases (e.g., N_2 herein). It is derived from the mobility measurement in the IMS drift tube, where ions with open conformation undergo more collisions with buffer gas molecules and hence travel more slowly than the

https://doi.org/10.5194/amt-2019-184
Preprint. Discussion started: 19 June 2019

Atmospheric Measurement Techniques Discussions

compact ones (Shvartsburg et al., 2000). Combination of collision cross section with molecular mass (as denoted by mass to charge ratio, *m/z*) provides a two-dimensional space for separation of species based on their size as well as geometry. We have shown that species of the same chemical class (e.g., amines, alcohols, and carboxylic acids) tend to situate as a narrow band and follow a unique trend line on the 2-D space (Zhang et al., 2016b). Here we demonstrate the presence of a $\Omega_{N_2} - m/z$ trend line for alkyl nitrates. Figure 3 shows that the measured Ω_{N_2} of the AN adducts, regardless of the AN molecular structures and types of anions that promote the adduct formation, appear along the $\Omega_{N_2} - m/z$ trend line predicted by the core model (deviations less than 5.2%). Also shown here are the predicted $\Omega_{N_2} - m/z$ trend lines for *mono*/*multi*-carboxylic acids and organic sulfates, which readily produce molecular ions via deprotonation ($[M\text{-}H]^-$) during negative ESI. Alkyl nitrates can be distinguished from carboxylic acids and sulfates based on their distinct collision cross sections vs. mass to charge ratio relationship. Note that other important chemical classes of atmospheric interest, such as amines, alcohols, aldehydes, and peroxides, are suitable for analysis in the positive ESI and their trend lines are not given here.

3.3. Characteristic fragments upon collision-induced dissociation

Molecular structures of selected AN ion adducts were further probed with the assistance of the collision-induced dissociation (CID) analysis, which was performed after the drift tube but prior to the time-of-flight chamber. The resulting daughter ion appears at the same drift time as the parent ion, allowing for a straightforward correlation of any given ion with its fragments. As shown in Figure 4, the nitrate ion (NO_3^-) at *m/z* 62 is exclusively observed upon CID of the parent ion adducts formed from MNG, DNG, and PETN by clustering with Cl^-, NO_3^-, and Ac^-. The NO_3^- fragment resulting from decomposition of the corresponding parent ion adduct can be well separated from that originally added to the AN solution based on their entirely different ion mobilities (as reflected by the measured drift time). Thus NO_3^- is considered as a characteristic fragment upon CID of the parent AN adduct ion and serves as a tracer to verify the presence of the $-ONO_2$ functional group in unknown compounds.

The anions (Cl^-, NO_3^-, and Ac^-) that promote the clustering chemistry were not observed upon CID of the parent AN adducts. Figure 5 shows the profiles of four ion adducts, i.e., $[MNG+Cl]^-$, $[MNG+Ac]^-$, $[PETN+Cl]^-$, and $[PETN+I]^-$, as well as their resulting fragments under a sequence of CID potential gradient. As expected, the abundance of the transmitted parent ion adducts decreases as the CID voltage rises. NO_3^-

https://doi.org/10.5194/amt-2019-184
Preprint. Discussion started: 19 June 2019

Atmospheric Measurement Techniques Discussions

appears as the largest product ion, and its enhanced abundance with increasing CID voltage is balanced by the decrease in signals of the corresponding parent ion adduct. Cl^- and Ac^- remain minor peaks over the entire range of displayed CID potential gradient. Under low-energy collisions, the parent AN ion adduct principally follows two fragmentation pathways, leading to either Cl^-/ Ac^-/I^- with the neutral AN molecule or the deprotonated AN molecular ion ($[M\text{-}H]^-$) via the neutral loss of HCl / HAc / HI. The absence of Cl^- and Ac^- indicates higher gas-phase basicity of Cl^- / Ac^- than $[M\text{-}H]^-$. As a result, the mechanism yielding $[M\text{-}H]^-$ is the dominant fragmentation pathway of AN ion adducts (with an exception for $[PETN+I]^-$). The resulting molecular ion $[M\text{-}H]^-$ decomposes promptly to NO_3^- due to the presence of the fragile R–ONO_2 bond.

3.4. Application to isoprene SOA

The OH-initiated oxidation of isoprene produces a population of isoprene peroxy radicals (RO_2), the fate of which depends on the level of nitric oxide. Under high-NO conditions as performed in the chamber experiments here, RO_2 radicals preferentially react with NO leading to major first-generation products including isoprene hydroxy nitrates, among which the two β-hydroxy nitrates dominate the isomer distribution. Due to the presence of a double bond, the hydroxy nitrate could undergo OH addition followed again by reactions of RO_2 radicals with NO, leading to a spectrum of products, of which some highly functionalized molecules such as the dihydroxy dinitrate are potential SOA precursors (Wennberg et al., 2018).

A pair of ion adducts at *m/z* 261 ($[M+^{35}Cl]^-$) and *m/z* 263 ($[M+^{37}Cl]^-$) with the abundance ratio of 3:1 is observed in the mass spectra of the isoprene SOA extracts in methanol with 0.2 mM sodium chloride as the additive. These two adducts share an identical mobility (DT = ~25.8 ms), which also appears as a small peak (DT = ~25.7 ms) in the mobility spectra of the NO_3^- ion (bottom panel of Figure 6). Further inspection of the 'mobility-selected' mass spectra of the parent ion adduct at *m/z* 261 reveals that NO_3^- is the major fragment ion (top panel of Figure 6). With the application of a CID potential sequence, the intensity of the precursor ion at *m/z* 261 decreases and that of the fragment ion at *m/z* 62 increases (middle panel of Figure 6), a similar pattern observed for the AN standards. We thereby tentatively assign the parent ion adduct at *m/z* 261 to a second-generation oxidation product, dihydroxy dinitrate ($C_5H_{10}O_8N_2$, see the chemical structure given in Figure 6), which is produced from the addition of OH to the two double bonds of isoprene followed by RO_2+NO reactions. It is interesting to note that a small shoulder peak appears at ~26.0 ms in the mobility spectra of the ion adduct at *m/z* 261 (bottom

https://doi.org/10.5194/amt-2019-184
Preprint. Discussion started: 19 June 2019

Atmospheric Measurement Techniques Discussions

panel of Figure 6), likely representative of the $C_5H_{10}O_8N_2$ isomers generated from the much less favored OH-addition channels that produce primary RO_2 radicals. Quantitative analysis of the dihydroxy dinitrate is complicated by the matrix interference during the ESI process and chromatographic separation prior to infusion to the ESI source is required (Zhang et al., 2015; Zhang et al., 2016a), which is beyond the capability of the current instrument setup. Further note that first-generation hydroxy nitrates were not detected, due to their relatively high volatility and thus quite limited partitioning onto the particle phase. On the other hand, multiple peaks were observed in the mobility spectra of the NO_3^- ion (bottom panel of Figure 6), and their drift times are higher than that of the ion assigned to the dihydroxy dinitrate, implying that some high-molecular-weight nitrate products were likely fragmented in the quadrupole interface.

4. Conclusions

The anion attachment chemistry was previously used in the negative ESI operation to effectively induce ion formation from neutral molecules that lack acidic sites (Zhu and Cole, 2000). Here we build upon the use of anion attachment, a special chemical ionization mechanism in solution, to characterize the condensed-phase alkyl nitrates at molecular level. The propensity of the $–ONO_2$ moiety to cluster with a diverse selection of anions, including Cl^-, I^-, NO_3^-, and Ac^-, was observed during the negative electrospray ionization process, and the measured total ion signals were enhanced by ultimately two orders of magnitude. Compared with conventional mass spectrometric techniques, the coupled ion mobility and mass-to-charge ratio measurements provide a two-dimensional separation of alkyl nitrates from other chemical classes commonly detected in negative ESI, such as organic sulfates and carboxylic acids. With the assistance of the collision-induced dissociation analysis, upon which the resulting product ions share the identical drift time as the precursor ion, molecular structures of ANs can be further probed. Regardless of the types of anions attached to the AN molecules, dissociation of the parent adduct ion yields a characteristic fragment, NO_3^- at *m/z* 62, which can be used to verify the presence of the $–ONO_2$ functional group in any given molecule. These new features enable the unambiguous identification of alkyl nitrates in a complex organic mixture, as exemplified by the detection of hydroxynitrates in isoprene derived SOA. The IMS-MS technique for the measurement of condensed-phase ANs is in its early stages of development. Accurate quantification of a given AN molecule by minimizing the ion suppression and improving the long-term stability of ESI is needed for future work.

https://doi.org/10.5194/amt-2019-184
Preprint. Discussion started: 19 June 2019

Atmospheric Measurement Techniques Discussions

Acknowledgements

The National Center for Atmospheric Research is operated by the University Corporation for Atmospheric Research, under the sponsorship of the National Science Foundation.

References

Atlas, E.: Evidence for≥ C3 alkyl nitrates in rural and remote atmospheres, Nature, 331, 426 - 428, 1988.

Beaver, M. R., St Clair, J. M., Paulot, F., Spencer, K. M., Crounse, J. D., LaFranchi, B. W., Min, K. E., Pusede, S. E., Wooldridge, P. J., and Schade, G. W.: Importance of biogenic precursors to the budget of organic nitrates: observations of multifunctional organic nitrates by CIMS and TD-LIF during BEARPEX 2009, Atmos. Chem. Phys., 12, 5773-5785, 2012.

Brown, S. S., Degouw, J. A., Warneke, C., Ryerson, T. B., Dubé, W. P., Atlas, E., Weber, R. J., Peltier, R. E., Neuman, J. A., and Roberts, J. M.: Nocturnal isoprene oxidation over the Northeast United States in summer and its impact on reactive nitrogen partitioning and secondary organic aerosol, Atmos. Chem. Phys., 9, 3027-3042, 2009.

Cech, N. B., and Enke, C. G.: Practical implications of some recent studies in electrospray ionization fundamentals, Mass Spectrom. Rev., 20, 362-387, 2001.

Day, D. A., Wooldridge, P. J., Dillon, M. B., Thornton, J. A., and Cohen, R. C.: A thermal dissociation laser ‐ induced fluorescence instrument for in situ detection of NO2, peroxy nitrates, alkyl nitrates, and HNO3, J. Geophys. Res. Atmos., 107, 2002.

Farmer, D. K., Matsunaga, A., Docherty, K. S., Surratt, J. D., Seinfeld, J. H., Ziemann, P. J., and Jimenez, J. L.: Response of an aerosol mass spectrometer to organonitrates and organosulfates and implications for atmospheric chemistry, Proc. Natl. Acad. Sci. USA, 107, 6670-6675, 2010.

Farmer, D. K., Perring, A. E., Wooldridge, P. J., Blake, D. R., Baker, A., Meinardi, S., Huey, L. G., Tanner, D., Vargas, O., and Cohen, R. C.: Impact of organic nitrates on urban ozone production, Atmos. Chem. Phys., 11, 4085-4094, 2011.

Groessl, M., Graf, S., and Knochenmuss, R.: High resolution ion mobility-mass spectrometry for separation and identification of isomeric lipids, Analyst, 140, 6904-6911, 2015.

Huang, D. D., Zhang, X., Dalleska, N. F., Lignell, H., Coggon, M. M., Chan, C. M., Flagan, R. C., Seinfeld, J. H., and Chan, C. K.: A note on the effects of inorganic seed aerosol on the oxidation state of secondary organic aerosol—α ‐ pinene ozonolysis, J. Geophys. Res. Atmos., 121, 12476-12483, 2016.

Kaplan, K., Graf, S., Tanner, C., Gonin, M., Fuhrer, K., Knochenmuss, R., Dwivedi, P., and Hill Jr, H. H.: Resistive Glass IM-TOFMS, Anal. Chem., 82, 9336-9343, 2010.

Kiendler-Scharr, A., Mensah, A. A., Friese, E., Topping, D., Nemitz, E., Prevot, A. S. H., Äijälä, M., Allan, J., Canonaco, F., and Canagaratna, M.: Ubiquity of organic nitrates

https://doi.org/10.5194/amt-2019-184
Preprint. Discussion started: 19 June 2019

Atmospheric Measurement Techniques Discussions

340 from nighttime chemistry in the European submicron aerosol, Geophys. Res. Lett., 43,
341 7735-7744, 2016.

342 Krechmer, J. E., Coggon, M. M., Massoli, P., Nguyen, T. B., Crounse, J. D., Hu, W.,
343 Day, D. A., Tyndall, G. S., Henze, D. K., Rivera-Rios, J. C., Nowak, J. B., Kimmel, J. R.,
344 III, R. L. M., Stark, H., Jayne, J. T., Sipila, M., Junninen, H., Clair, J. M. S., Zhang, X.,
345 Feiner, P. A., Zhang, L., Miller, D. O., Brune, W. H., Keutsch, F. N., Wennberg, P. O.,
346 Seinfeld, J. H., Worsnop, D. R., Jimenez, J. L., and Canagaratna, M. R.: Formation of
347 low volatility organic compounds and secondary organic aerosol from isoprene
348 hydroxyhydroperoxide low-NO oxidation, Environ. Sci. Technol., 49, 10330-10339,
349 2015.

350 Krechmer, J. E., Groessl, M., Zhang, X., Junninen, H., Massoli, P., Lambe, A. T.,
351 Kimmel, J. R., Cubison, M. J., Graf, S., Lin, Y. H., Budisulistiorini, S. H., Zhang, H.,
352 Surratt, J. D., Knochenmuss, R., Jayne, J. T., Worsnop, D. R., Jimenez, J. L., and
353 Canagaratna, M. R.: Ion mobility spectrometry–mass spectrometry (IMS–MS) for on-
354 and offline analysis of atmospheric gas and aerosol species, Atmos. Meas. Tech., 9,
355 3245-3262, 2016.

356 Lee, B. H., Mohr, C., Lopez-Hilfiker, F. D., Lutz, A., Hallquist, M., Lee, L., Romer, P.,
357 Cohen, R. C., Iyer, S., and Kurtén, T.: Highly functionalized organic nitrates in the
358 southeast United States: Contribution to secondary organic aerosol and reactive nitrogen
359 budgets, Proc. Natl. Acad. Sci. USA, 113, 1516-1521, 2016.

360 Loza, C. L., Craven, J. S., Yee, L. D., Coggon, M. M., Schwantes, R. H., Shiraiwa, M.,
361 Zhang, X., Schilling, K. A., Ng, N. L., and Canagaratna, M. R.: Secondary organic
362 aerosol yields of 12-carbon alkanes, Atmos. Chem. Phys., 14, 1423-1439, 2014.

363 Nguyen, T. B., Bates, K. H., Crounse, J. D., Schwantes, R. H., Zhang, X., Kjaergaard, H.
364 G., Surratt, J. D., Lin, P., Laskin, A., and Seinfeld, J. H.: Mechanism of the hydroxyl
365 radical oxidation of methacryloyl peroxynitrate (MPAN) and its pathway toward
366 secondary organic aerosol formation in the atmosphere, Phys. Chem. Chem. Phys., 17,
367 17914-17926, 2015.

368 O'Brien, J. M., Shepson, P. B., Muthuramu, K., Hao, C., Niki, H., Hastie, D. R., Taylor,
369 R., and Roussel, P. B.: Measurements of alkyl and multifunctional organic nitrates at a
370 rural site in Ontario, J. Geophys. Res. Atmos., 100, 22795-22804, 1995.

371 Perring, A. E., Pusede, S. E., and Cohen, R. C.: An observational perspective on the
372 atmospheric impacts of alkyl and multifunctional nitrates on ozone and secondary
373 organic aerosol, Chem. Rev., 113, 5848-5870, 2013.

374 Rollins, A. W., Smith, J. D., Wilson, K. R., and Cohen, R. C.: Real time in situ detection
375 of organic nitrates in atmospheric aerosols, Environ. Sci. Technol., 44, 5540-5545, 2010.

376 Rollins, A. W., Browne, E. C., Min, K. E., Pusede, S. E., Wooldridge, P. J., Gentner, D.
377 R., Goldstein, A. H., Liu, S., Day, D. A., and Russell, L. M.: Evidence for NOx control
378 over nighttime SOA formation, Science, 337, 1210-1212, 2012.

379 Rosen, R. S., Wood, E. C., Wooldridge, P. J., Thornton, J. A., Day, D. A., Kuster, W.,
380 Williams, E. J., Jobson, B. T., and Cohen, R. C.: Observations of total alkyl nitrates

https://doi.org/10.5194/amt-2019-184
Preprint. Discussion started: 19 June 2019

during Texas Air Quality Study 2000: Implications for O3 and alkyl nitrate photochemistry, J. Geophys. Res. Atmos., 109, 2004.

Russell, L. M., Bahadur, R., and Ziemann, P. J.: Identifying organic aerosol sources by comparing functional group composition in chamber and atmospheric particles, Proc. Natl. Acad. Sci. USA, 108, 3516-3521, 2011.

Schilling Fahnestock, K. A., Yee, L. D., Loza, C. L., Coggon, M. M., Schwantes, R., Zhang, X., Dalleska, N. F., and Seinfeld, J. H.: Secondary organic aerosol composition from C12 alkanes, J. Phys. Chem. A, 119, 4281-4297, 2014.

Schwantes, R. H., Teng, A. P., Nguyen, T. B., Coggon, M. M., Crounse, J. D., St. Clair, J. M., Zhang, X., Schilling, K. A., Seinfeld, J. H., and Wennberg, P. O.: Isoprene NO3 Oxidation Products from the RO2+ HO2 Pathway, J. Phys. Chem. A, 119, 10158-10171, 2015.

Schwantes, R. H., Schilling, K. A., McVay, R. C., Lignell, H., Coggon, M. M., Zhang, X., Wennberg, P. O., and Seinfeld, J. H.: Formation of highly oxygenated low-volatility products from cresol oxidation, Atmos. Chem. Phys., 17, 3453-3474, 2017.

Shvartsburg, A. A., Liu, B., Jarrold, M. F., and Ho, K.-M.: Modeling ionic mobilities by scattering on electronic density isosurfaces: Application to silicon cluster anions, J. Chem. Phys., 112, 4517-4526, 2000.

Teng, A. P., Crounse, J. D., Lee, L., St Clair, J. M., Cohen, R. C., and Wennberg, P. O.: Hydroxy nitrate production in the OH-initiated oxidation of alkenes, Atmos. Chem. Phys., 15, 4297-4316, 2015.

Thomas, D. A., Coggon, M. M., Lignell, H., Schilling, K. A., Zhang, X., Schwantes, R. H., Flagan, R. C., Seinfeld, J. H., and Beauchamp, J. L.: Real-time studies of iron oxalate-mediated oxidation of glycolaldehyde as a model for photochemical aging of aqueous tropospheric aerosols, Environ. Sci. Technol., 50, 12241-12249, 2016.

Thornton, J. A., Wooldridge, P. J., and Cohen, R. C.: Atmospheric NO2: In situ laser-induced fluorescence detection at parts per trillion mixing ratios, Anal. Chem., 72, 528-539, 2000.

Wooldridge, P. J., Perring, A. E., Bertram, T. H., Flocke, F. M., Roberts, J. M., Singh, H. B., Huey, L. G., Thornton, J. A., Wolfe, G. M., and Murphy, J. G.: Total Peroxy Nitrates (ΣPNs) in the atmosphere: the Thermal Dissociation-Laser Induced Fluorescence (TD-LIF) technique and comparisons to speciated PAN measurements, Atmos. Meas. Tech., 3, 593-607, 2010.

Xiong, F., McAvey, K. M., Pratt, K. A., Groff, C. J., Hostetler, M. A., Lipton, M. A., Starn, T. K., Seeley, J. V., Bertman, S. B., and Teng, A. P.: Observation of isoprene hydroxynitrates in the southeastern United States and implications for the fate of NO x, Atmos. Chem. Phys., 15, 11257-11272, 2015.

Xu, W., Croteau, P., Williams, L., Canagaratna, M., Onasch, T., Cross, E., Zhang, X., Robinson, W., Worsnop, D., and Jayne, J.: Laboratory characterization of an aerosol chemical speciation monitor with PM2. 5 measurement capability, Aerosol Sci. Tech., 51, 69-83, 2017.

https://doi.org/10.5194/amt-2019-184
Preprint. Discussion started: 19 June 2019


Atmospheric Measurement Techniques Discussions

422 Zhang, X., Schwantes, R. H., Coggon, M. M., Loza, C. L., Schilling, K. A., Flagan, R.
423 C., and Seinfeld, J. H.: Role of ozone in SOA formation from alkane photooxidation,
424 Atmos. Chem. Phys., 14, 1733-1753, 2014.

425 Zhang, X., McVay, R. C., Huang, D. D., Dalleska, N. F., Aumont, B., Flagan, R. C., and
426 Seinfeld, J. H.: Formation and evolution of molecular products in α-pinene secondary
427 organic aerosol, Proc. Natl. Acad. Sci. USA, 112, 14168-14173, 2015.

428 Zhang, X., Dalleska, N. F., Huang, D. D., Bates, K. H., Sorooshian, A., Flagan, R. C.,
429 and Seinfeld, J. H.: Time-resolved molecular characterization of organic aerosols by
430 PILS+ UPLC/ESI-Q-TOFMS, Atmos. Environ., 130, 180-189, 2016a.

431 Zhang, X., Krechmer, J. E., Groessl, M., Xu, W., Graf, S., Cubison, M., Jayne, J. T.,
432 Jimenez, J. L., Worsnop, D. R., and Canagaratna, M. R.: A novel framework for
433 molecular characterization of atmospherically relevant organic compounds based on
434 collision cross section and mass-to-charge ratio, Atmos. Chem. Phys., 16, 12945-12959,
435 2016b.

436 Zhang, X., Lambe, A. T., Upshur, M. A., Brooks, W. A., Gray Bé, A., Thomson, R. J.,
437 Geiger, F. M., Surratt, J. D., Zhang, Z., and Gold, A.: Highly oxygenated multifunctional
438 compounds in α-pinene secondary organic aerosol, Environ. Sci. Technol., 51, 5932-
439 5940, 2017.

440 Zhang, X., Ortega, J., Huang, Y., Shertz, S., Tyndall, G. S., and Orlando, J. J.: A steady-
441 state continuous flow chamber for the study of daytime and nighttime chemistry under
442 atmospherically relevant NO levels, Atmos. Meas. Tech., 11, 2537-2551, 2018.

443 Zhu, J., and Cole, R. B.: Formation and decompositions of chloride adduct ions,[M+
444 Cl]−, in negative ion electrospray ionization mass spectrometry, J. Am. Soc. Mass
445 Spectrom., 11, 932-941, 2000.

446

447

448

449

450

451

452

453

454

455

456

https://doi.org/10.5194/amt-2019-184
Preprint. Discussion started: 19 June 2019

Atmospheric Measurement Techniques Discussions

457 Table 1. Overview of compounds containing $–ONO_2$ and $–NO_2$ functional groups
458 investigated in this study.

Compound	Molecular Formula	Ion Formula	Ion *m/z*	LOD [a] (μM)	Ω_{N_2} [b] (Å^2)	Structure
1-Mononitroglycerin (MNG)	$C_3H_7NO_5$	$[M+Cl]^-$	172.0	0.8	129.4	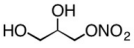
		$[M+NO_2\text{-}H]^-$	182.0	0.7	132.7	
		$[M+Ac]^-$	196.0	0.3	139.2	
1,3-Dinitroglycerin (DNG)	$C_3H_6N_2O_7$	$[M+Cl]^-$	217.0	1.1	151.1	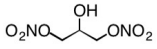
		$[M+NO_2\text{-}H]^-$	227.0	4.3	156.6	
		$[M+NO_3]^-$	244.0	0.6	151.7	
		$[M+I]^-$	308.9	0.8	177.0	
Pentaerythritol tetranitrate (PETN)	$C_5H_8N_4O_{12}$	$[M-H]^-$	315.0	1.1	181.7	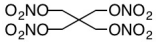
		$[M+Cl]^-$	351.0	0.5	183.7	
		$[M+NO_2\text{-}H]^-$	361.0	0.9	190.7	
		$[M+NO_3]^-$	378.0	0.2	190.9	
		$[M+I]^-$	442.9	0.1	216.2	
		$[2M+Cl]^-$	667.0	1.0	262.6	
2,4-Dinitrotoluene (DNT)	$C_7H_6N_2O_4$	$[M-H]^-$	181.0	0.6	137.0	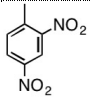
Hexahydro-1,3,5-trinitro-1,3,5-triazine (RDX)	$C_3H_6N_6O_6$	$[M+Cl]^-$	257.0	0.3	149.8	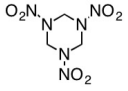
		$[M+NO_2\text{-}H]^-$	267.1	1.4	156.3	
		$[M+NO_3]^-$	284.0	0.2	160.8	
		$[M+I]^-$	348.9	0.1	181.9	
		$[2M+Cl]^-$	479.0	1.6	203.5	

[a] The limit of detection (LOD) is calculated as LOD = σ×(S/N)/*k*, where S/N is the signal-to-noise ratio, which is taken as 3 here, *k* is the response factor of IMS-MS towards individual ion adducts produced from 5 μM standard nitrate solution during negative ESI, and σ is the standard deviation of the IMS-MS response over the course of 60 s measurements.

[b] The collision cross section (Ω_{N_2}) is calculated through the modified zero field (so called Mason-Schamp) equation, see more details in Zhang et al. (2016).

459
460
461
462
463

https://doi.org/10.5194/amt-2019-184
Preprint. Discussion started: 19 June 2019

Atmospheric Measurement Techniques Discussions

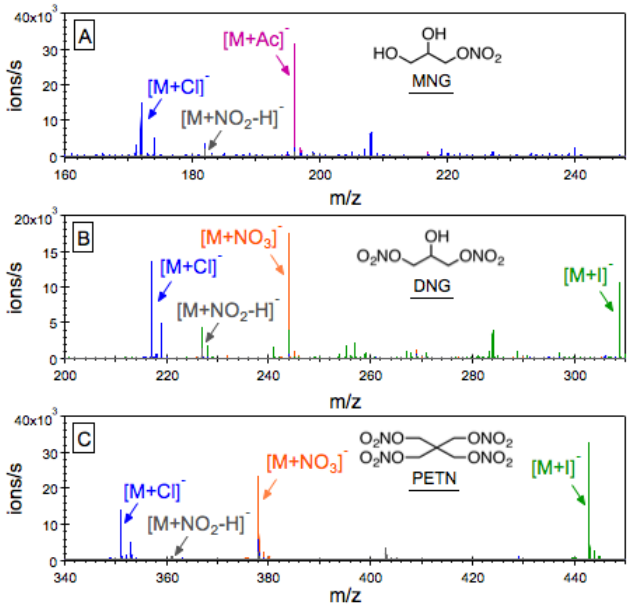

Figure 1. Negative ESI mass spectra of 5 µM 1-mononitroglycerin (MNG), 1,3-dinitroglycerin (DNG), and pentaerythritol tetranitrate (PETN) dissolved in pure methanol (gray), methanol with 0.1 mM ammonium acetate (NH_4Ac, purple), methanol with 0.1 mM ammonium chloride (NH_4Cl, blue), methanol with 0.1 mM sodium nitrate ($NaNO_3$, orange), and methanol with 0.1 mM sodium iodide (NaI, green). These three alkyl nitrates, which do not readily produce significant amount of molecular ions on their own during negative ESI, are observed as clusters with acetate (Ac^-), chloride (Cl^-), nitrate (NO_3^-), and iodide anions (I^-) in the ESI(–) spectra.

https://doi.org/10.5194/amt-2019-184
Preprint. Discussion started: 19 June 2019

Atmospheric Measurement Techniques Discussions

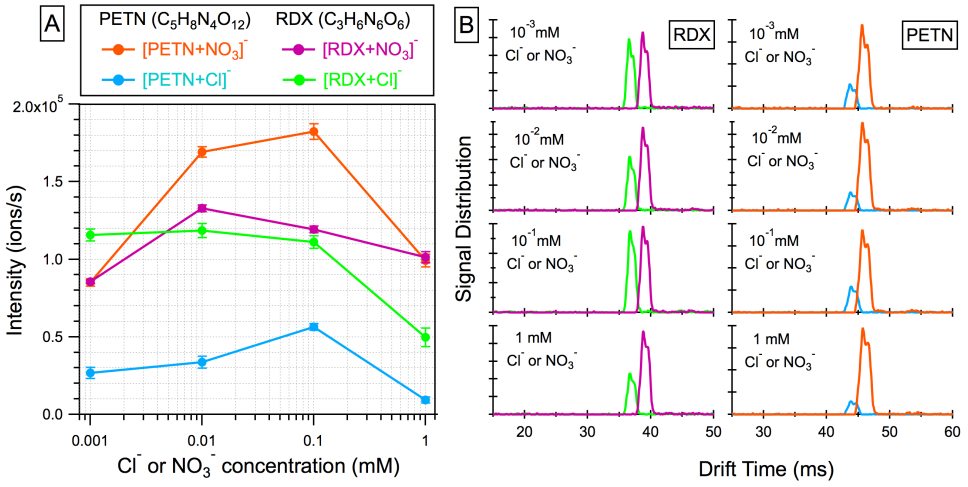

Figure 2. (A) Signals of the ion adducts produced from RDX and PETN by clustering with chloride (Cl^-) and nitrate (NO_3^-) as a function of the corresponding anion concentrations ranging from 1 μM to 1 mM. (B) Drift time distributions of the ion adducts $[RDX+Cl]^-$, $[PETN+Cl]^-$, $[RDX+NO_3]^-$, and $[PETN+NO_3]^-$ are consistent at different anion concentrations.

https://doi.org/10.5194/amt-2019-184
Preprint. Discussion started: 19 June 2019

Atmospheric Measurement Techniques Discussions

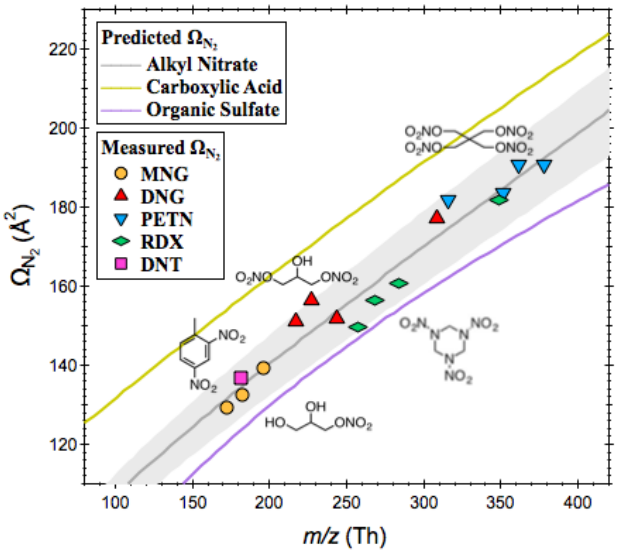

Figure 3. Measured collision cross sections (Ω_{N_2}) of the AN ion adducts as a function of their mass-to-charge ratios appear along the predicted Ω_{N_2} – *m/z* trend line. Also shown here are the predicted Ω_{N_2} – *m/z* trend lines for carboxylic acids and organic sulfates, which are major chemical classes of atmospheric interest detected in the negative ESI mode.

https://doi.org/10.5194/amt-2019-184
Preprint. Discussion started: 19 June 2019

Atmospheric Measurement Techniques Discussions

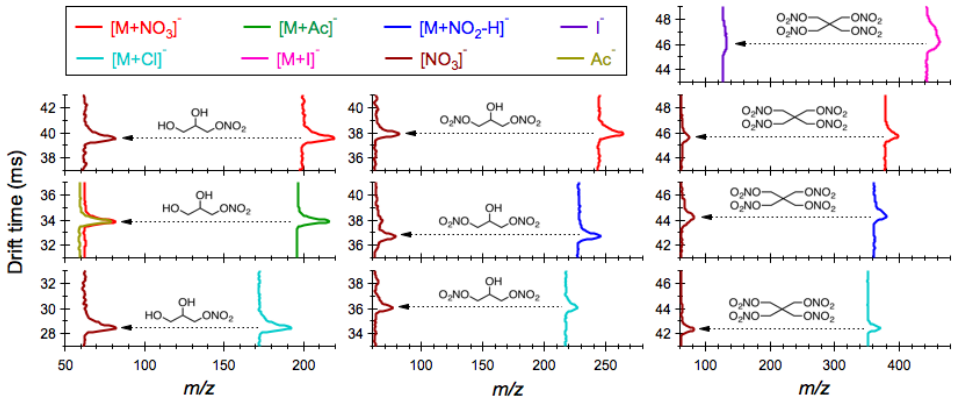

Figure 4. Characteristic fragment ions produced from MNG, DNG, and PETN by clustering with acetate (Ac^-), chloride (Cl^-), iodide (I^-), nitrate (NO_3^-), and nitrite (NO_2^-) upon collision induced dissociation performed at a CID voltage of 20 V.

https://doi.org/10.5194/amt-2019-184
Preprint. Discussion started: 19 June 2019

Atmospheric Measurement Techniques Discussions

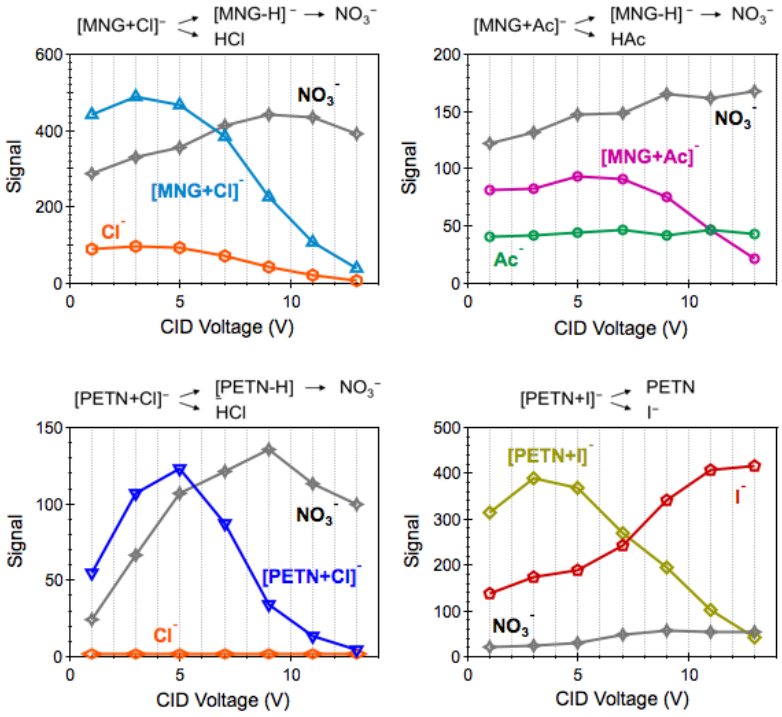

Figure 5. Peak intensities of the precursor ion adducts $[MNG+Cl]^-$, $[MNG+Ac]^-$, $[PETN+Cl]^-$, and $[PETN+I]^-$ as well as their fragment ions as a function of the collision energy as displayed by the CID voltage.

https://doi.org/10.5194/amt-2019-184
Preprint. Discussion started: 19 June 2019

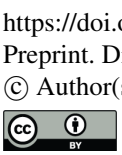

Atmospheric Measurement Techniques Discussions

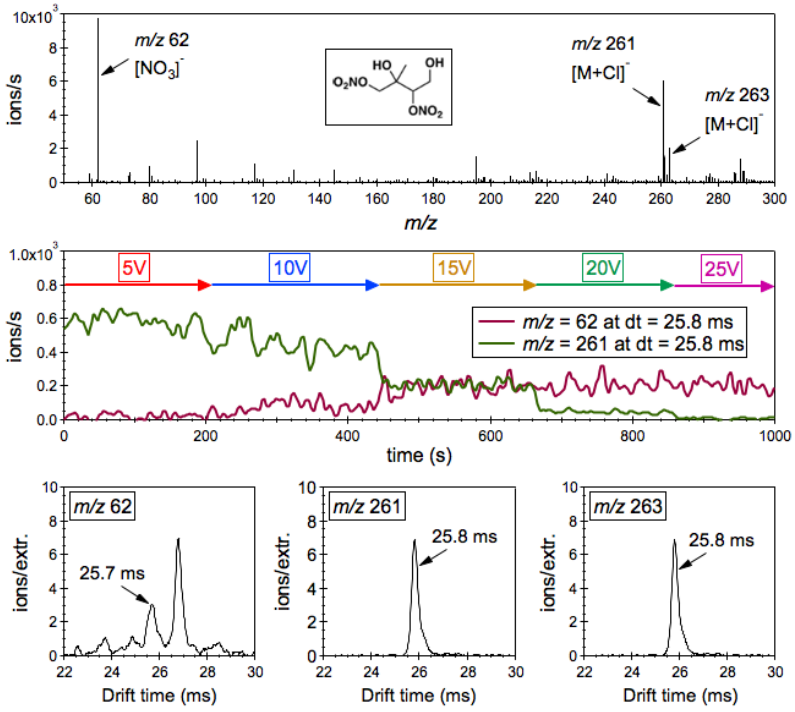

Figure 6. (Top panel) The 'mobility-selected' mass spectra of the parent ion adduct at *m/z* 261 and its major fragment at *m/z* 62 in isoprene SOA extracts with ~0.2 mM sodium chloride as the additive. (Middle panel) Profiles of the precursor ion adduct at *m/z* 261 and its product ion at *m/z* 62 as a function of the CID voltage. (Bottom panel) Drift time spectra of the ion adduct at *m/z* 261, its isotope ion adduct at *m/z* 263, and the fragment ion at *m/z* 62.